Electrochemical Behavior of Copper Complexes with Substituted Polypyridinic Ligands: An Experimental and Theoretical Study

Walter Cañon-Mancisidor, Evgenia Spodine, and Diego Venegas-Yazigi*

Departamento de Química Inorgánica y Analítica, Facultad de Ciencias Químicas y Farmacéuticas, CIMAT, Universidad de Chile, Olivos 1007, Santiago, Chile

Darío Rojas and Jorge Manzur*

Departamento de Ciencia de los Materiales, Facultad de Ciencias Físicas y Matemáticas, Universidad de Chile, Tupper 2069, Santiago, Chile

Santiago Alvarez

Departamento de Química Inorgànica i Centre de Recerca en Química Teòrica, Universitat de Barcelona, Barcelona, Spain

Experimental redox potentials of the couples $[Cu(R-L^n)(CH_3CN)]^{2+,+}$, where L^1 is bis-(pyridine-2-ylmethyl)-benzylamine, L^2 is (pyridine-2-ylethyl)(pyridine-2-ylmethyl)-benzylamine, and R is H, Me, or CF_3, were determined in dichloromethane solution. The compounds exhibited one simple quasi-reversible wave over the measured potential range of –500 to +1200 mV, and the $E_{1/2}$ values varied from +200 to +850 mV versus SCE. These experimental values were correlated with redox potentials calculated using density functional theory. The optimized geometries and the predicted redox potentials were obtained using the BP86 functional and a combination of the basis sets LACV3P** (for Cu) and cc-pVTZ(-f) (for light atoms). A distortion analysis of all of the optimized geometries for both oxidation states was performed using the generalized interconversion coordinate φ. A linear relation was obtained between this parameter and the redox potentials. However, the $[Cu(CF_3-L^1)(CH_3CN)]^+$ complex showed the largest deviation, which was explained by the more-rigid structure of the ligand.

Introduction

Redox potentials for different series of biomimetic Cu(II)/Cu(I) complexes with different ligands have been extensively studied in copper chemistry.[1–3] Correlations between the redox potentials and the nature of the donor atoms of the ligands have been reported.[4–6] For example, ligands containing both unsaturated nitrogen atoms and thioether sulfur atoms have been shown to facilitate the reduction of Cu(II) to Cu(I).[7] The effect of coordination geometry on the redox potentials of copper complexes has been investigated since Karlin suggested that copper sites in metalloproteins exhibit geometries that favor the Cu(I) oxidation state.[8] The nature and number of substituents have also been shown to affect the value of the redox potentials of the Cu(II)/Cu(I) couple.[9,10] This kind of analysis has been done for different types of copper complexes, since the redox properties of these species can be used to rationalize their reactivities

* To whom correspondence should be addressed. E-mail: dvy@uchile.cl (D.V.-Y.), jmanzur@dqb.uchile.cl (J.M.).

(1) Kitajima, N.; Morooka, Y. *Chem. Rev.* **1994**, *94*, 737–757.
(2) Ambundo, E. A.; Deydier, M.; Grall, A. J.; Aguera-Vega, N.; Dressel, L. T.; Cooper, T. H.; Hegg, M. J.; Ochrymowyez, L. A.; Rorabacher, D. B. *Inorg. Chem.* **1999**, *38*, 4233–4242.
(3) Rorabacher, D. B. *Chem. Rev.* **2004**, *104*, 651–697.
(4) Dockal, E.; Jones, T. E.; Sokol, W. F.; Engerer, R. J.; Rorabacher, D. B.; Ochrymowyez, L. A. *J. Am. Chem. Soc.* **1976**, *98*, 4322–2324.
(5) Patterson, G. S.; Holm, R. H. *Bioinorg. Chem.* **1975**, *4*, 257–275.
(6) Addison, A. W. *Inorg. Chim. Acta* **1989**, *162*, 217–220.

toward oxygen.[11,12] In all of the mentioned examples, the discussion has been related to the correlation of the electrochemical behavior with the solid-state structure obtained using X-ray diffraction.[13–15] However, using solid-state structure parameters to correlate with electrochemical behavior may give incorrect correlations, since the geometry in solution could be quite different from that in the solid state. This makes theoretical determination of the solution-phase structure an important issue.

Moreover, theoretical prediction of redox potentials permits many catalytic processes and electrochemical mechanisms to be understood. However, theoretical prediction has been undertaken less frequently than existing experimental correlations.[16–20] One of the first studies involving the prediction of redox potentials of organic molecules was the work done by Winget et al.,[17] who used the B3LYP hybrid functional and the cc-pVTZ(-f) basis set. Complexes with first- and second-row transition-metal ions were studied by Baik et al.[16] using the same hybrid functional but a different basis set [cc-pVTZ(-f) for light atoms and LACV3P** for metal atoms]. Uudsemaa et al.[18] also calculated redox potentials for complexes of first-row transition metal ions, using a gradient-corrected functional (BP86) with the LACVP* basis set.

In this work, experimental redox potentials were determined for the couples $[Cu(R-L^n)(CH_3CN)]^{2+,+}$, where L^1 is bis-(pyridine-2-ylmethyl)-benzylamine, L^2 is (pyridine-2-ylethyl)(pyridine-2-ylmethyl)-benzylamine, and R is H, Me, or CF_3. The experimental values were correlated with calculated redox potentials. Several calculation methods were used in order to reproduce the experimental redox potentials. A shape parameter that takes into account the percentage of distortion between two perfect geometries was correlated with theoretical and experimental redox potentials.[21]

Experimental Section

Commercially available reagent-grade reagents and solvents were used, unless otherwise stated.

^{1}H NMR spectra were recorded in $CDCl_3$ using a Bruker AMX-300 NMR spectrometer. Chemical shifts are reported as δ values downfield from an internal Me_4Si reference. Cyclic voltammetry measurements were made using a BAS CV-50W instrument at a scan rate of 100 mV s^{-1} in a three-electrode cell having a glassy carbon electrode as the working electrode, a platinum wire as the auxiliary electrode, and a saturated calomel electrode (SCE) as the reference electrode. Tetra-*n*-butylammonium perchlorate (0.1 M) was used as the supporting electrolyte. Solutions (1 mM) of the copper(I) complexes in dichloromethane (freshly distilled from calcium hydride) were made in situ by directly mixing the proper amounts (77 μL and 1 mmol, respectively) of a $Cu(AN)_4ClO_4$ solution (0.13 M) in acetonitrile (AN) and the corresponding ligand in the cell (10 cm^3 total volume) under nitrogen. All of the potentials are reported versus SCE at a scan rate of 100 mV s^{-1}.

Syntheses. The ligands bis(pyridine-2-ylmethyl)-benzylamine ($H-L^1$), (6-methylpyridine-2-ylmethyl)(pyridine-2-ylmethyl)-benzylamine ($Me-L^1$), (pyridine-2-ylmethyl)(6-trifluoromethyl-pyridine-2-ylmethyl)-benzylamine (CF_3-L^1), (pyridine-2-ylethyl)(pyridine-2-ylmethyl)-benzylamine ($H-L^2$), and (pyridine-2-ylethyl)(6-trifluoromethyl-pyridine-2-ylmethyl)-benzylamine (CF_3-L^2) were prepared according to a literature procedure by reaction of the appropriate secondary amine with benzyl bromide in CH_3CN as the solvent.[22] (6-Methylpyridine-2-ylethyl)(pyridine-2-ylmethyl)-benzylamine ($Me-L^2$) was not obtained in its pure form, and therefore, the corresponding voltammetric studies were not performed. Structures of the ligands are shown schematically in Scheme 1.

^{1}H NMR Data. $H-L^1$: 3.68 (s, 2H, Ph$-CH_2$), 3.81 (s, 4H, Py$-CH_2$), 7.13–8.51 (several multiplets, 13H, phenyl and pyridine protons).

$Me-L^1$: 2.52 (s, 3H, CH_3), 3.68 (s, 2H, Ph$-CH_2$), 3.78 (s, 2H, R$-$Py$-CH_2$), 3.81 (s, 2H, Py$-CH_2$), 7.0–8.52 (several multiplets, 12H, phenyl and pyridine protons).

CF_3-L^1: 3.71 (s, 2H, Ph$-CH_2$), 3.83 (s, 2H, Py$-CH_2$), 3.88 (s, 2H, R$-$Py$-CH_2$), 7.1–8.53 (several multiplets, 12H, phenyl and pyridine protons).

$H-L^2$: 3.0 (dt, 4H, CH_2-CH_2), 3.65 (s, 2H, Ph$-CH_2$), 3.82 (s, 2H, Py$-CH_2$), 7.1–8.5 (several multiplets, 13H, phenyl and pyridine protons).

CF_3-L^2: 2.9 (dt, 4H, CH_2-CH_2), 3.6 (s, 2H, Ph$-CH_2$), 3.8 (s, 2H, R$-$Py$-CH_2$), 7.1–8.5 (several multiplets, 12H, phenyl and pyridine protons).

Computational Details. The structures were fully optimized in the gas and solvent phases using density functional theory (DFT) under an unrestricted approximation. Two different functionals (B3LYP and BP86[23–27]) and three different basis sets [LACVP*, LACV3P**, and cc-pVTZ(-f)[28–30]] were tested in order to find the best functional and basis set to use in calculating the redox potentials for these systems. On the basis of absolute deviations, the BP86 functional and the basis sets cc-pVTZ(-f) (for light atoms) and LACV3P** (for Cu) were selected (see Table S1 in the Supporting Information). A continuous solvent model based on

(11) Schatz, M.; Becker, M.; Thaler, F.; Hampel, F.; Schindler, S.; Jacobson, R. R.; Tyeklár, Z.; Murthy, N. N.; Ghosh, P.; Chen, Q.; Zubieta, J.; Karlin, K. D. *Inorg. Chem.* **2001**, *40*, 2312–2322.
(12) Mizuno, M.; Hayashi, H.; Fujinami, S.; Furutachi, H.; Nagamoto, S.; Otake, S.; Uozumi, K.; Suzuki, M.; Kitagawa, T. *Inorg. Chem.* **2003**, *42*, 8534–8544.
(13) Nagao, H.; Komeda, N.; Mukaida, M.; Suzuki, M.; Tanaka, K. *Inorg. Chem.* **1996**, *35*, 6809–6815.
(14) Zhao, X.; Nilges, M. J.; Lu, Y. *Biochemistry* **2005**, *44*, 6559–6564.
(15) Libeu, C. A. P.; Kukimoto, M.; Nishiyama, M.; Horinouchi, S.; Adman, E. T. *Biochemistry* **1997**, *36*, 13160–13179.
(16) Baik, M. H.; Friesner, R. A. *J. Phys. Chem. A* **2002**, *106*, 7407–7412.
(17) Winget, P.; Weber, E. J.; Cramer, C. J.; Truhlar, D. G. *Phys. Chem. Chem. Phys.* **2000**, *2*, 1231–1239.
(18) Uudsemaa, M.; Tamm, T. *J. Phys. Chem. A* **2003**, *107*, 9997–10003.
(19) Winget, P.; Cramer, C. J.; Truhlar, D. G. *Theor. Chem. Acc.* **2004**, *112*, 217–227.
(20) Shimodaira, Y.; Miura, T.; Kudo, A.; Kobayashi, H. *J. Chem. Theory Comput.* **2007**, *3*, 789–795.
(21) Alvarez, S.; Alemany, P.; Casanova, D.; Cirera, J.; Llunell, M.; Avnir, D. *Coord. Chem. Rev.* **2005**, *249*, 1693–1708.
(22) Rojas, D.; García, A. M.; Vega, A.; Moreno, Y.; Venegas-Yazigi, D.; Garland, M. T.; Manzur, J. *Inorg. Chem.* **2004**, *43*, 6324–6330.
(23) Becke, A. D. *J. Chem. Phys.* **1993**, *98*, 5648–5652.
(24) Becke, A. D. *Phys. Rev. A* **1988**, *38*, 3098–3100.
(25) Lee, C. T.; Wang, W. T.; Parr, R. G. *Phys. Rev. B* **1988**, *37*, 785–789.
(26) Vosko, S. H.; Wilk, L.; Nusair, M. *Can. J. Phys.* **1980**, *58*, 1200–1211.
(27) Slater, J. C. *Quantum Theory of Molecules and Solids, Vol. 4: The Self-Consistent Field for Molecules and Solids*; McGraw-Hill: New York, 1974.
(28) Hay, P. J.; Wadt, W. R. *J. Chem. Phys.* **1985**, *82*, 299–310.
(29) The LACV3P basis set is a triple-ζ contraction of the LACVP basis set developed and tested at Schrödinger, Inc.
(30) Dunning, T. H., Jr. *J. Chem. Phys.* **1989**, *90*, 1007–1023.

Scheme 1. Schematic Drawing of the Ligands Used in This Study

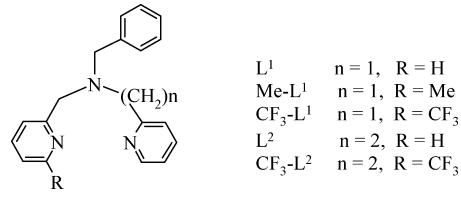

Scheme 2. Vertical and Adiabatic Redox Processes

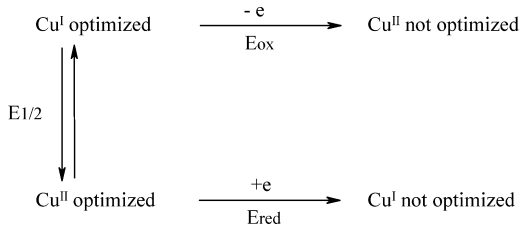

Scheme 3. Thermodynamic Cycle for the Oxidation Process

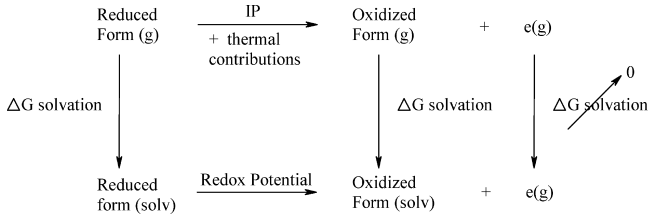

numerical solution of the Poisson−Boltzmann equation[31] was used. All of the DFT calculations were performed using the Jaguar 5.5 code.[32] Distortion analyses for the calculated geometries of the complexes were performed within the framework of Avnir's continuous shape measures[39,40] using the SHAPE code.[33]

Prediction of Redox Potentials. Theoretical redox potentials were calculated using either a vertical or an adiabatic process (Scheme 2). Vertical transitions differ from adiabatic ones in that the former permit calculation of the reduction and oxidation potentials (E_{red} and E_{ox}, respectively) while the latter allow estimation of the half-potential ($E_{1/2}$).

Scheme 3 shows a free-energy-based thermodynamic cycle for both processes. Experimental redox potentials are always reported relative to a reference potential, typically the normal hydrogen electrode (NHE). In the case of theoretical redox potentials, this convention then refers to the free-energy change for the net reaction resulting from addition of the NHE half-reaction to the value of the free-energy cycle. The free-energy change associated with the NHE half-reaction is –4.28 eV.[34] Thus, the redox potential in solution can be obtained from Scheme 3. In order to obtain the redox potentials referred to SCE, –0.24 eV must be added.[35] A detailed description of Scheme 3 is given by Winget et al.[17]

Results and Discussion

Electrochemistry. The copper(I) complexes were prepared in situ by mixing an acetonitrile solution of $Cu(AN)_4^+$ with the corresponding ligand in a 1:1 molar ratio in dichloromethane (see the Experimental Section). These experimental conditions allowed the assumption that the tetracoordinated cuprous species $[Cu(R-L^n)(CH_3CN)]^+$ was present in solution. Cyclic voltammetry experiments showed that the stepwise addition of the ligand to the copper(I) solution results in the partial formation of the copper complex. Thus, at a copper-to-ligand ratio of 1:0.5, only half of the copper(I) was converted to the complex, as can be observed from the cyclic voltammogram (CV) of the resulting solution (Figure S1b in the Supporting Information), which showed two signals, one corresponding to the $[Cu(AN)_4]^+$ species and the other to the $[Cu(R-L^n)]^+$ complex. On the other hand, at a copper-to-ligand ratio of 1:1, the CV (Figure S1a in the Supporting Information) exhibited only the signal corresponding to the $[Cu(R-L^n)]^+$ complex.

Table 1. Experimental Redox Potentials (mV vs SCE) for the $[Cu(R-L^n)(CH_3CN)]^+$ Complexes in CH_2Cl_2

complex	experimental E_a	experimental E_c	$E_{1/2}$	ΔE
$[Cu(H-L^1)(CH_3CN)]^+$	0.305	0.221	0.263	0.084
$[Cu(Me-L^1)(CH_3CN)]^+$	0.561	0.407	0.484	0.154
$[Cu(CF_3-L^1)(CH_3CN)]^+$	0.698	0.579	0.638	0.119
$[Cu(H-L^2)(CH_3CN)]^+$	0.410	0.295	0.352	0.115
$[Cu(CF_3-L^2)(CH_3CN)]^+$	0.810	0.706	0.758	0.104

Table 1 shows the experimental potentials versus SCE and the peak-to-peak separations (ΔE = 80−150 mV) for the studied complexes. The compounds exhibited one simple quasi-reversible wave over the measured potential range from –500 to +1200 mV. The ratio of the anodic and cathodic peak currents was almost unity for all of the compounds except $[Cu(CF_3-L^2)(CH_3CN)]^+$, whose ratio was smaller. This ratio also changed with the scan rate, showing a lower reversibility in the latter case (Figure S2 in the Supporting Information). $E_{1/2}$ values for the studied compounds varied from +200 to +850 mV versus SCE. A typical CV scan for $[Cu(H-L^1)(CH_3CN)]^+$ is given in Figure 1.

Variable scan rate experiments showed that slower scan rates gave slightly smaller peak separations, but the scans were never electrochemically reversible. The inset in Figure 1 shows the scan-rate dependence of the observed CV for compound $[Cu(H-L^1)(CH_3CN)]^+$. Even though the CV suggests a quasi-reversible process, cycling of the oxidation and reduction did not significantly decrease the signal intensities, consistent with a slow ligand rearrangement to accommodate the preferred coordination geometry of each oxidation state of the copper center. It would appear that the quasi-reversibility is due to molecular reorganization when Cu(I) is oxidized to Cu(II) and vice versa.

The influence of ligand flexibility on the electrochemical behavior of a series of tetradentate tripodal tripyridylalkylamine ligands was studied by Schatz et al.,[11] who showed that an increase in ligand arm length (i.e., an increase in chelate ring size) results in an increase of the redox potential. The redox potential differences in the those systems were interpreted as arising from the difference in stability constants for Cu(II)−tripodal species. These studies have shown that Cu(II) favors chelation involving five-membered rings; therefore, compounds containing shorter arms are stabilized in higher oxidation states. Each change of the size of a

(31) The solvation calculation was performed using Jaguar's Poisson−Boltzmann solver.
(32) *Jaguar*, version 5.5; Schrödinger, LLC: Portland, OR, 2003.
(33) Llunell, M.; Casanova, D.; Cirera, J.; Bofill, J. M.; Alemany, P.; Alvarez, S.; Pinsky, M.; Avnir, D. *SHAPE*, version 1.1; Barcelona, Spain, 2003.
(34) Kelly, C. P.; Cramer, C. J.; Truhlar, D. G. *J. Phys. Chem. B* **2007**, *111*, 408–422.
(35) Bard, J.; Faulkner, L. R. *Electrochemical Methods*; Wiley: New York, 1980.

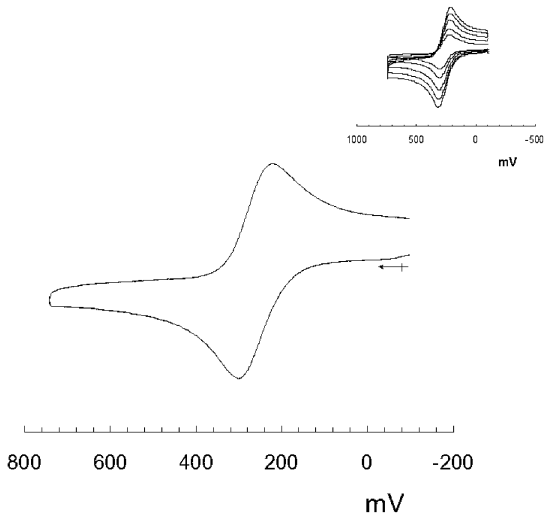

Figure 1. Cyclic voltammogram of $[Cu(H-L^1)(CH_3CN)]^+$. Inset: scan-rate dependence of the peak separation and intensity.

Scheme 4. Numbering of the Atoms of the First Coordination Sphere

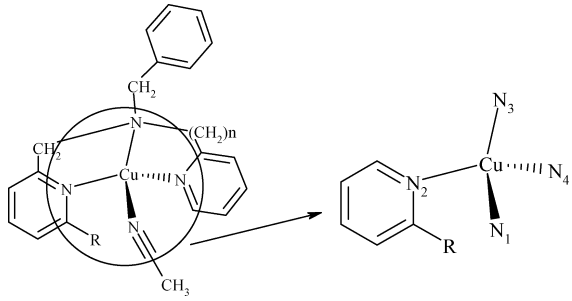

chelate ring in the complex from five to six members results in an increase of the Cu(II)−Cu(I) redox potential. The behavior of the previously studied complexes[11] is similar to that described above. In the systems studied in the present work, changing the size of the chelating ring from five to six also results in an increase of the redox potential.

In terms of the substituent effect, Nagao et al.[13] performed a structural and electrochemical comparison of Cu(II) complexes with methyl-substituted tetradentate tripodal tripyridylalkylamine ligands. They found that the redox potential of the Cu(II)/Cu(I) couple is primarily controlled by the molecular structure of the complexes, which depends on the number of methyl substituents present in the ligand. The introduction of a methyl or trifluoromethyl substituent at the 6-position of the reported ligands produced an increase in the redox potential, even though the electronic effects of these two groups are very different. This last result confirmed the influence of steric constraints on the redox potential.

Structural Analysis. The assumed tetrahedral structures of the copper(I) and copper(II) complexes were optimized, and distorted tetrahedral geometries were obtained. Scheme 4 shows that the first coordination sphere corresponds to three nitrogen atoms (two pyridinic and one aminic) from the ligand and one from the acetonitrile molecule. Tables 2 and 3 show selected bond distances and angles.

The copper−nitrogen distances calculated in this work for both copper(I) and copper(II) complexes with aminopyridine ligands are in good agreement with distances reported in the literature for solid-state structures. For similar copper complexes whose structures were obtained using X-ray diffraction,[11,22,36,37] the Cu−N(pyridine) distances are on the order of 2.00−2.05 Å, while our calculated distances are 1.98−2.02 Å. The Cu−N(amine) distances reported in the literature are in the range 2.02−2.21 Å, while our calculated values are 2.07−2.12 Å. The calculated $Cu-N_1$ distances corresponding to the acetonitrile molecule are also in the range 1.98−2.08 Å, as are the experimental values for the metal−solvent distance.[36,37]

Table 2. Calculated Cu−N Bond Distances (Å) for the Complexes $[Cu(R-L^n)(CH_3CN)]^+$ and $[Cu(R-L^n)(CH_3CN)]^{2+}$

complex	$Cu-N_1$	$Cu-N_2$	$Cu-N_3$	$Cu-N_4$
$[Cu(CF_3-L^2)(CH_3CN)]^+$	2.03	2.08	2.11	1.97
$[Cu(CF_3-L^2)(CH_3CN)]^{2+}$	2.04	2.01	2.12	1.97
$[Cu(H-L^2)(CH_3CN)]^+$	2.03	1.99	2.08	1.97
$[Cu(H-L^2)(CH_3CN)]^{2+}$	2.03	1.99	2.09	1.98
$[Cu(Me-L^2)(CH_3CN)]^+$	2.08	1.97	2.10	1.98
$[Cu(Me-L^2)(CH_3CN)]^{2+}$	2.07	1.98	2.10	1.97
$[Cu(CF_3-L^1)(CH_3CN)]^+$	1.98	2.02	2.11	1.99
$[Cu(CF_3-L^1)(CH_3CN)]^{2+}$	1.99	2.02	2.12	1.98
$[Cu(H-L^1)(CH_3CN)]^+$	1.98	2.00	2.11	1.99
$[Cu(H-L^1)(CH_3CN)]^{2+}$	1.99	2.01	2.07	1.99
$[Cu(Me-L^1)(CH_3CN)]^+$	1.98	2.02	2.07	2.00
$[Cu(Me-L^1)(CH_3CN)]^{2+}$	1.99	2.03	2.09	2.01

Table 3. Selected Calculated Angles (deg) for the Complexes $[Cu(R-L^n)(CH_3CN)]^+$ and $[Cu(R-L^n)(CH_3CN)]^{2+}$

complex	N_1-Cu-N_3	N_2-Cu-N_4
$[Cu(CF_3-L^2)(CH_3CN)]^+$	118.15	138.68
$[Cu(H-L^2)(CH_3CN)]^+$	137.26	148.73
$[Cu(Me-L^2)(CH_3CN)]^+$	122.61	150.81
$[Cu(CF_3-L^1)(CH_3CN)]^+$	118.19	140.25
$[Cu(H-L^1)(CH_3CN)]^+$	137.40	148.82
$[Cu(Me-L^1)(CH_3CN)]^+$	122.13	150.92
$[Cu(CF_3-L^2)(CH_3CN)]^{2+}$	120.72	123.74
$[Cu(H-L^2)(CH_3CN)]^{2+}$	158.54	143.53
$[Cu(Me-L^2)(CH_3CN)]^{2+}$	147.21	134.99
$[Cu(CF_3-L^1)(CH_3CN)]^{2+}$	122.23	125.67
$[Cu(H-L^1)(CH_3CN)]^{2+}$	158.83	143.82
$[Cu(Me-L^1)(CH_3CN)]^{2+}$	149.17	136.21

For each Cu(I) complex in the series studied in this work, the calculated Cu−N(amine) distance is longer than the other Cu−N distances in the same complex. This has also been observed experimentally.[36,37]

For each of the $[Cu(R-L^2)(CH_3CN)]^+$ and $[Cu(R-L^2)(CH_3CN)]^{2+}$ complexes, the Cu−N distance to the pyridine of the shorter arm is longer than the Cu−N distance to the pyridine of the longer arm. The substituent effect produces a change in this distance that depends on both the inductive and steric effects. For both of the complexes $[Cu(CF_3-L^2)(CH_3CN)]^+$ and $[Cu(CF_3-L^2)(CH_3CN)]^{2+}$, the steric and inductive effects produce an elongation of the Cu−N bond. For the two methyl-substituted complexes, $[Cu(Me-L^2)(CH_3CN)]^+$ and $[Cu(Me-L^2)(CH_3CN)]^{2+}$, the inductive effect increases the basicity of the pyridine nitrogen, which should produce a decrease in the Cu−N distance. One can also expect the steric effect to induce an increase in this distance. These two opposing effects should

(36) Osako, T.; Terada, S.; Tosha, T.; Nagatomo, S.; Furutachi, H.; Fujinami, S.; Kitagawa, T.; Suzuki, M.; Itoh, S. *Dalton Trans.* **2005**, 3514–3521.
(37) Osako, T.; Tachi, Y.; Taki, M.; Fukuzumi, S.; Itoh, S. *Inorg. Chem.* **2001**, *40*, 6604–6609.

Table 4. Path Deviation Function Δ(T−SP) and Generalized Interconversion Coordinate φ(T−SP) (Relative to the Distortion Path between the Tetrahedron and the Square) for the Studied Complexes[a]

complex	Δ(T−SP)	φ(T−SP)
$[Cu(H-L^1)(CH_3CN)]^+$	3	63
$[Cu(Me-L^1)(CH_3CN)]^+$	5	52
$[Cu(CF_3-L^1)(CH_3CN)]^+$	12	35
$[Cu(H-L^2)(CH_3CN)]^+$	2	50
$[Cu(Me-L^2)(CH_3CN)]^+$	4	42
$[Cu(CF_3-L^2)(CH_3CN)]^+$	6	33
$[Cu(H-L^1)(CH_3CN)]^{2+}$	3	62
$[Cu(Me-L^1)(CH_3CN)]^{2+}$	5	54
$[Cu(CF_3-L^1)(CH_3CN)]^{2+}$	11	36
$[Cu(H-L^2)(CH_3CN)]^{2+}$	2	50
$[Cu(Me-L^2)(CH_3CN)]^{2+}$	4	42
$[Cu(CF_3-L^2)(CH_3CN)]^{2+}$	6	34

[a] All values in percent.

combine to produce a small change in the Cu−N distance compared with that of the unsubsituted complexes. For the L^1 series, the observed changes in the Cu−N distances were smaller than those observed for the L^2 series, which can be attributed to the greater rigidity of the L^1 ligand.

All of the complexes have been shown to have distorted geometries. The distortions from an ideal geometry in a given structure can be quantified in terms of a generalized interconversion coordinate, φ, that indicates the percentage of distortion along the pathway from the ideal geometry to an alternative ideal structure, as defined by Alvarez et al.[33] In our study, φ reflects the deviation from the ideal tetrahedron (T) along two alternative distortion paths, one leading toward the square planar (SP) geometry and the other toward the vacant trigonal bipyramidal (vTBP) geometry. It must be noted, however, that the interconversion coordinate is meaningful only if the structure under consideration is along the minimal distortion path between the two reference geometries, as indicated by the value of the path deviation function, Δ.[38] Both the path deviation function and the generalized interconversion coordinate are calculated in a straightforward way from the continuous shape measures[39,40] obtained from atomic coordinates through the SHAPE program.[33]

Values of φ for the studied complexes are shown in Table 4. All of our structures were located along the path between the tetrahedral and the square planar geometries, since all of the calculated deviation function values were less than 6% except for the values of 12 and 11% for $[Cu(CF_3-L^1)(CH_3CN)]^+$ and $[Cu(CF_3-L^1)(CH_3CN)]^{2+}$, respectively. The deviation function values calculated for the distortion path from the ideal tetrahedron to the ideal vacant trigonal bipyramid were dramatically larger for the complete series (Table S2 in the Supporting Information), thus ruling out this distortion mode for the compounds under study. Consequently, the generalized interconversion coordinate from the tetrahedral to the square planar geometry permits us to adequately describe the distortions present in our complexes.

Calculated Redox Potentials. Detailed results obtained for the calculated redox potentials using different functionals and basis sets are shown in Table S3 in the Supporting Information. The use of two basis sets, one for the ligand and one for the metal center, improved the final outcome of the calculation. The redox potentials predicted using the B3LYP/LACV3P**/cc-pVTZ(-f) and BP86/LACV3P**/cc-pVTZ(-f) methods gave better approximations to the experimental values than those calculated using B3LYP/LACVP* or BP86/LACVP*. For both the adiabatic and vertical processes, analysis of the average absolute deviations showed that the BP86/LACV3P**/cc-pVTZ(-f) method was best; it gave better results for the vertical process (see Tables S1, S3, and S4 in the Supporting Information).

Table 5. Experimental and Calculated Oxidation and Reduction Potentials for $[Cu(R-L^n)(CH_3CN)]^+$ and $[Cu(R-L^n)(CH_3CN)]^{2+}$ Complexes (R = CF_3, Me, H; n = 1, 2)

	potential (V)	
	experimental	calculated[a]
oxidation		
$[Cu(CF_3-L^2)(CH_3CN)]^+$	0.810	0.838
$[Cu(H-L^2)(CH_3CN)]^+$	0.410	0.459
reduction		
$[Cu(CF_3-L^2)(CH_3CN)]^{2+}$	0.706	0.638
$[Cu(H-L^2)(CH_3CN)]^{2+}$	0.295	0.307
oxidation		
$[Cu(CF_3-L^1)(CH_3CN)]^+$	0.698	1.015
$[Cu(H-L^1)(CH_3CN)]^+$	0.305	0.347
$[Cu(Me-L^1)(CH_3CN)]^+$	0.561	0.611
reduction		
$[Cu(CF_3-L^1)(CH_3CN)]^{2+}$	0.579	0.858
$[Cu(H-L^1)(CH_3CN)]^{2+}$	0.221	0.208
$[Cu(Me-L^1)(CH_3CN)]^{2+}$	0.407	0.421

[a] Calculated using the BP86/LACV3P**/cc-pVTZ(-f) method.

Because the cyclic voltammetry experiments were performed in CH_2Cl_2, which is a noncoordinating solvent, and showed good reversibility (ΔE = 84 to 151 mV), we could assume that the same coordination sphere around the copper center existed for both oxidation states. Osako et al.[37] reported a similar four-coordinate complex (having an acetonitrile molecule in the first coordination sphere) whose CV in dichloromethane solution exhibited a peak separation of 170 mV. The authors considered this good reversibility to indicate that the acetonitrile ligand was maintained during the electrochemical process. Since even better reversibility (smaller peak separation) has been observed in the present study, we also assumed essentially the same coordination environment for both copper oxidation states. Table 5 gives the best calculated oxidation and reduction potentials for the studied complexes. Good correlation between the experimental and calculated values can be observed (Figure 2a,b).

For both correlations shown in Figure 2, it is possible to observe that the $[Cu(CF_3-L^1)(CH_3CN)]^{2+,+}$ couple deviates from the general tendency. This can be rationalized by considering that the calculated distortion parameters for these complexes indicate a nonpure tetrahedral−square planar distortion, as discussed above. This distortion may be due to the rigid character of the CF_3-L^1 ligand, which could allow the bonding of an extra acetonitrile molecule and therefore a modification from tetra- to pentacoordinate geometry that would stabilize the copper(II) oxidation state. As the theoretical modeling considered both species to exist

(38) Casanova, D.; Cirera, J.; Llunell, M.; Alemany, P.; Avnir, D.; Alvarez, S. *J. Am. Chem. Soc.* **2004**, *126*, 1755–1763.
(39) Zabrodsky, H.; Peleg, S.; Avnir, D. *J. Am. Chem. Soc.* **1992**, *114*, 7843–7851.
(40) Pinsky, M.; Avnir, D. *Inorg. Chem.* **1998**, *37*, 5575–5582.

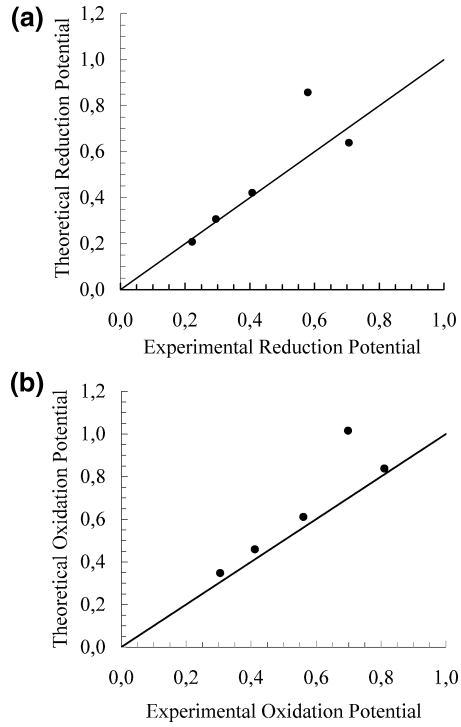

Figure 2. Correlation between the theoretical and experimental (a) reduction and (b) oxidation potentials.

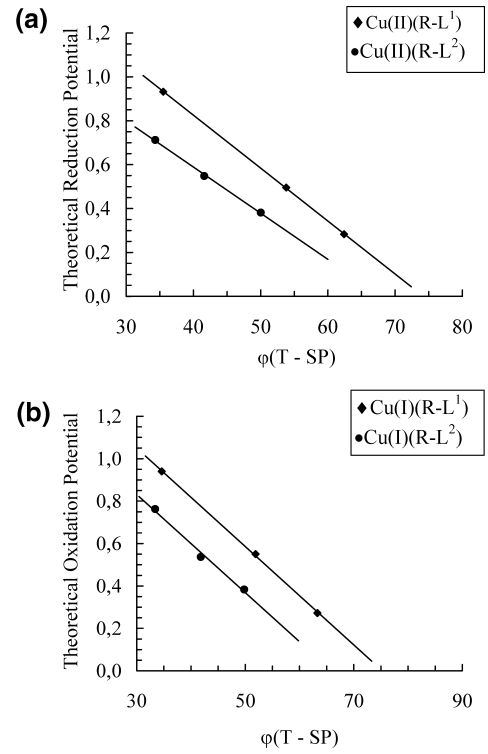

Figure 3. Correlation between the calculated (a) reduction and (b) oxidation potentials and the generalized interconversion coordinate φ(T−SP).

in a tetracoordinate environment, the calculated redox potentials deviate from the experimental values.

The redox potentials can clearly be seen to depend on the coordination geometry of the copper ions when they are plotted as functions of the generalized interconversion coordinate, φ(T−SP), as shown in panels a and b of Figure 3 for reduction and oxidation potentials, respectively. For each family of complexes with the same ligand, the reduction potentials decrease as the Cu(II) complexes become more distorted from the tetrahedron (Figure 3a). Similarly, the oxidation potentials for each family decrease with increased planarization of the Cu(I) coordination geometry (Figure 3b). Finally, it is interesting to point out that the linear relationships between the calculated redox potential and the parameter φ for the two series $[Cu(R-L^1)(CH_3CN)]^{2+,+}$ and $[Cu(R-L^2)(CH_3CN)]^{2+,+}$ show similar slopes, as can be observed in Figure 3a,b.

Conclusions

Here we have presented the results of an experimental and theoretical study of the electrochemical behavior of a family of copper complexes with polypyridinic ligands. The experimental values of the redox potentials were rationalized by both steric and electronic substituent effects. The BP86/LACV3P**/cc-pVTZ(-f) calculation method gave the best approximation to the experimental potential values. The generalized interconversion coordinate, φ, was shown to be a good descriptor of the distortion produced by the substituent and oxidation-state effects. A linear relationship between this parameter and the redox potentials was obtained. However, the $[Cu(CF_3-L^1)(CH_3CN)]^+$ complex showed the largest deviation, which was explained in terms of the more-rigid structure of the ligand.

Acknowledgment. The authors thank the FONDECYT 1050484 and FONDAP 11980002 projects for financial support. W.C.-M. thanks CIMAT for a scholarship, and D.V.-Y. thanks Proyecto Bicentenario de Inserción Académica and Proyecto DI-UChile INI06/08-2.

Supporting Information Available: Average absolute deviations for the vertical and adiabatic processes (Table S1), path deviation functions relative to the T−SP and T−vTBP distortions for the studied complexes (Table S2), theoretical and experimental redox potentials of complexes obtained from vertical and adiabatic processes (Tables S3 and S4, respectively), CVs for the formation of complexes in Cu(I)-to-ligand molar ratios of 1:1 and 1:0.5 (Figure S1), and CVs at different scan rates for a typical complex (Figure S2). This material is available free of charge via the Internet at http://pubs.acs.org.

IC702104U